Published in final edited form as:

Retina. 2016 December ; 36(Suppl 1): S12–S25. doi:10.1097/IAE.0000000000001276.

Visualizing retinal pigment epithelium phenotypes in the transition to geographic atrophy in age-related macular degeneration

Emma C. Zanzottera, MD[1,2,*], **Thomas Ach, MD**[1,3,*], **Carrie Huisingh, MPH**[4], **Jeffrey D. Messinger, DC**[1], **Richard F. Spaide, MD**[5], and **Christine A. Curcio, PhD**[1]

[1]Department of Ophthalmology, University of Alabama School of Medicine, Birmingham, Alabama USA

[2]Eye Clinic, Department of Clinical Science “Luigi Sacco”, Sacco Hospital, University of Milan, Milan, Italy

[3]University Hospital Würzburg, Department of Ophthalmology, Würzburg, Germany

[4]Department of Epidemiology, School of Public Health; University of Alabama at Birmingham; Birmingham, Alabama

[5]Vitreous Retina Macula Consultants of New York

Abstract

Purpose—To inform the interpretation of clinical optical coherence tomography and fundus autofluorescence?imaging in geographic atrophy (GA) of age-related macular degeneration (AMD) by determining the distribution of retinal pigment epithelium (RPE) phenotypes in the transition from health to atrophy (GA) in donor eyes.

Method—In RPE-Bruch’s membrane flat mounts of 2 GA eyes the terminations of organized RPE cytoskeleton and autofluorescent material were compared. In high-resolution histological sections of 13 GA eyes, RPE phenotypes were assessed at ±500 and ±100 μm from the descent of the external limiting membrane (ELM) towards Bruch’s membrane. The ELM descent was defined as curved, reflected, or oblique in shape. Thicknesses of RPE, basal laminar deposit (BLamD), and RPE+BLamD were measured.

Results—A border of atrophy that can be precisely delimited is the ELM descent, as opposed to the termination of the RPE layer itself, because of dissociated RPE in the atrophic area. Approaching the ELM descent, the percentage of abnormal RPE morphologies increases, the percentage of age-normal cells decreases, overall RPE thickens, and BLamD does not thin. The combination of RPE plus BLamD is 19.7% thicker at −100 μm from the ELM descent than at −500 μm (23.1 ± 10.7 vs 19.3 ± 8.2 μm; p=0.05).

Corresponding Address: Christine A. Curcio, PhD; Department of Ophthalmology; EyeSight Foundation of Alabama Vision Research Laboratories; 1670 University Boulevard Room 360, University of Alabama School of Medicine; Birmingham AL 35294-0099; Ph 205.996.8682; F 205.934.3425; curcio@uab.edu.

*Authors should be considered co-first

Conclusion—The distribution of RPE phenotypes at the GA transition support the idea that these morphologies represent defined stages of a degeneration sequence. The idea RPE dysmorphia including rounding and stacking helps explain variable autofluorescence patterns in GA [14] is reinforced. The ELM descent and RPE+BLamD thickness profile may have utility as SDOCT metrics in clinical trials.

Précis

Morphological phenotypes of the retinal pigment epithelium distribute across the transition to atrophy in age-related macular degeneration in a manner consistent with a recently described two-pathway hypothesis of RPE fate and also reinforce RPE dysmorphia as a candidate mechanism for variable autofluorescence.

Keywords

Age-related macular degeneration; retinal pigment epithelium; geographic atrophy; histology; optical coherence tomography; autofluorescence; external limiting membrane

Introduction

Geographic atrophy (GA) in end-stage age-related macular degeneration (AMD) is a loss of retinal pigment epithelium (RPE) as revealed by clinical imaging modalities that highlight RPE organelles (lipofuscin, melanolipofuscin, melanosomes). GA expansion is orderly and quantifiable, and it is an important endpoint for clinical trials. [1,2] Because the fate of cells at the transition between health and atrophy may be irreversible despite intervention, understanding cellular and molecular changes in this region is requisite for validating GA enlargement as an endpoint. Precursors of atrophy are also desirable, both for monitoring disease progression and severity and for illuminating disease mechanisms that might enable earlier intervention. [3–6] Because imaging technologies currently used to define GA are critically affected by the morphology of individual RPE cells, the transition to GA can be newly informed with data from high-resolution and comprehensive histology. [7–9]

Fundus autofluorescence (FAF) is an imaging technique dependent on stimulated emission of light, mostly from RPE lipofuscin, a lysosomal organelle containing bis-retinoid by-products of the visual cycle and other non-degradable material. [10, 11] Absence of FAF signal is taken to indicate RPE atrophy although the exact margins of hypo-FAF have not been topographically correlated with the margin of RPE loss in any published series. Hyper-FAF is posited as an indicator for progression in GA by natural history studies[12], with different FAF patterns indicating different expansion rates. [12, 13] Hyper-FAF can be explained by several cell-autonomous mechanisms, including increased concentration of efficiently detected fluorophores, increased concentration of lipofuscin granules, loss or re-positioning of melanosomes, RPE dysmorphia resulting in taller individual cells, and RPE migration resulting in vertically superimposed cells. [14, 15] In a histologic study of 10 GA eyes, using unbiased sampling, quantification of autofluorescence (AF), and a grading system for RPE morphology, [14] we determined that hyperautofluorescence could be explained by enlargement and stacking of cells that created a longer path length for exciting light through fluorophores, rather than a high intracellular concentration of lipofuscin granules.

The transition to atrophy exhibits a degeneration sequence in which space serves a surrogate for time. Previous histopathologic studies of the GA transition (Supplementary Table 1) described cells of irregular shape and pigmentation, sloughed and heaped cells, cells in double layers, and RPE-derived material within the neurosensory retina. [14–17] Sarks et al [18] reported a steady progression of worsening RPE morphology towards the atrophic area, which we confirmed. [14] To define an RPE stress-response repertoire in AMD, we recently used high-resolution histology to create a taxonomy of morphologic phenotypes using spindle-shaped melanosomes as markers. Phenotypes were then assembled into a schema of plausible transitions [7, 8] that suggested two main pathways of RPE fate. One pathway comprises sloughing of spherical pigmented cells into the subretinal space with anterior migration into the neurosensory retina. A second pathway comprises ‘shedding’ of granule aggregates into underlying basal laminar deposits (BLamD) in a manner consistent with apoptosis. [9, 14] Following migration and death, the remaining epithelium disintegrates into fully pigmented ‘dissociated’ cells scattered across atrophic areas. [7, 8, 19] Dissociated RPE cells in turn are sources of ‘subducted’ cells found between the RPE basal lamina and Bruch membrane. These newly described migratory cells of apparent RPE origin play an as-yet undefined role in AMD progression. Remarkably, most RPE phenotypes are visible by SDOCT, [8, 20, 21] suggesting that an accurate timeline of RPE degeneration is attainable through clinical imaging.

Here we tested whether RPE phenotypes [7–9] distribute across the GA transition in a manner consistent with the two-pathway hypothesis of RPE fate described in the previous paragraph. We demonstrate numerous AF and pigmented RPE in the atrophic zone. We describe progression and clearing on either side of an atrophy border defined by the descent of the external limiting membrane (ELM) towards Bruch’s membrane. Our data support the two-pathway model and reinforce RPE dysmorphia as a strong candidate mechanism for variable FAF.

Methods

RPE flat mounts of AMD eyes were studied to assess the relationship of AF and cytoskeleton at the termination of the intact RPE layer, as described. [9] In other AMD eyes, sub-micrometer histological cross-sections through the fovea and superior perifovea were studied to assess phenotypes of RPE morphology, as described. [7, 8] All tissues were taken from a bio-repository of short post-mortem (<6 hr) eyes assembled for AMD research from donors to the Alabama Eye Bank in 1995–2009. Our studies were approved by institutional review at the University of Alabama at Birmingham and adhered to the Tenets of the Declaration of Helsinki.

Flat-mounts

Of 35 RPE-Bruch’s membrane flat-mounts previously prepared from 35 Caucasian donors, [9] 2 GA tissues were revisited. AMD status was determined at the time of accession using stereo color photographs from a dissecting microscope, based on criteria of the Alabama Age- related Maculopathy Grading System. [22] The presence of atrophic areas was also verified in *ex vivo* AF imaging (Spectralis, Heidelberg Engineering, Heidelberg, Germany).

To enable definition of the RPE cytoskeleton, F-actin was labeled with Alexa 647 phalloidin (Life Technologies, Grand Island, NY, USA). To illustrate RPE cell melanosome content and to illustrate F-actin and lipofuscin/melanolipofuscin distribution, bright field and fluorescence imaging, respectively, was performed using a confocal microscope (BX51, Olympus, Center Valley, PA, USA) at predefined locations and settings, as described, plus additional locations in areas affected by atrophy. [23]

Cross-sectional histology

Of 82 AMD eyes prepared for sub-micrometer epoxy sections stained with toluidine blue, 13 eyes with GA from 12 donors (8 women, 4 men, 85.6 ± 4.9 years) were identified by absence of a continuous RPE layer for a distance >250 μm in the presence of basal linear deposit or drusen and in the absence of evidence of neovascularization.

We identified the descent of the ELM towards Bruch's membrane, as detailed in the Results section. At 100 μm and 500 μm on either side of this boundary, in agreement with previous clinical studies, [24–26] we annotated RPE morphology and measured RPE and BLamD thickness, for a total of 4 assessments per transition (2 in the atrophic area and 2 in the non-atrophic area). Negative distances (−500 and −100 μm) represent locations on the non-atrophic side of the ELM descent, and positive distances (+100 and +500 μm) are on the atrophic side, so that progression moves like a time-line from left (non-atrophic) to right (atrophic) in all figures. This sampling pattern, centered around a defined point, differs from that in our previous publications, also using these eyes, which spaced samples systematically across the whole macula. [7, 8] Annotations were recorded in a custom database (Filemaker) while using a 60X numerical aperture = 1.4 objective and CCD camera to display tissue images at 1900X on a monitor (in the range of low magnification electron microscopy). We used the nomenclature for RPE morphology defined by Zanzottera et al [7, 8] (Table 1). In brief, cells containing spindle-shaped melanosomes and lipofuscin apposed to a basal lamina or basal laminar deposits were considered RPE and cells in other layers or spaces containing those organelles or plausibly derived from such cells, were considered RPE-derived. The percentage of each RPE morphology was referenced to the total number of samples with RPE (which differs from our previous studies [7, 8]).

Our results are based on the analysis of 13 eyes of 12 donors, 18 sections (13 central, 5 superior), 69 transitions, and 171 assessment locations (36 at −500 μm, 63 at −100 μm, 47 at +100 μm, 25 at +500 μm). The number and pattern of assessment locations differed among eyes, because atrophic areas extended off section edges, were less than 1000 μm wide, or did not extend into the superior macula.

We compared mean RPE thickness for each phenotype at −500 μm and −100 μm and mean BLamD thickness at ±500 μm and ±100 μm. Per previous convention, [7, 8] only cells in the RPE layer (and not pigmented cells out of the layer) were measured. Also by convention, thicknesses at sites of 'sloughed' included two cells if the migrating cell was touching cells in the layer and just the epithelial cell if it was not. RPE thicknesses were available for all RPE morphologies except 'atrophy with' and 'without BLamD' and 'dissociated' RPE. Generalized estimating equations were used to test if the mean thickness of RPE (or BLamD) at each location was different from zero. A pooled variance was used so that a p-

value could be generated even if only one observation was included in one of the groups. A *p*-value <0.05 was considered statistically significant.

Results

In flat-mounts we compared the termination of intact RPE layer, signified by orderly cytoskeleton delimiting polygonal cells, to the distribution of AF attributable to lipofuscin and melanolipofuscin. Figure 1 shows multiple cells in the area beyond an organized RPE mosaic, consistent with the numerous spherical and fully pigmented cells found atop BLamD and Bruch's membrane in late AMD eyes by cross-sectional histology and adaptive optics assisted imaging. [7, 8, 15, 19] In addition, by demonstrating directly that the atrophy border is not sharply defined in the RPE layer itself by histology, these data prompt us to seek a more reliable reference point for analyzing the sequence of degeneration.

Guided by an early description by S.H. Sarks, [27] we chose as a marker of the atrophy border the descent of the external limiting membrane (ELM) towards Bruch's membrane. The ELM comprises junctional complexes between the Müller cells and photoreceptor inner segments [28–30] and together with junctional complexes among RPE, bounds the subretinal space. [31] Figures 2 and 3 show high-magnification and low-magnification histologic views, respectively, of three GA eyes, demonstrating how the ELM descent assumes one of three shapes: curved as originally described [27] (Figure 2A), oblique (Figure 2B), and reflected (Figure 2C). The outer nuclear layer can parallel the ELM in its course to end coterminously with the ELM descent (Figure 3B), or it can sweep further into the atrophic area (Figure 3A,C). On the non-atrophic side of curved and reflected ELM descents (Figure 3A,C), individual photoreceptors (and the Müller cells interleaved among them) shorten and shift orientations from vertical and orthogonal to Bruch's membrane to horizontal and parallel to Bruch's membrane. The atrophic area delimited by the ELM descent contains a small number of cone photoreceptor cell bodies (lacking outer segments and wave-guiding capability), either as part of outer retinal tubulation [32–35] or as part of the outer nuclear layer where it diverges horizontally from the ELM (Figure 3A,C). Thus the ELM descent cleanly divides a region where photoreceptors are present and potentially salvageable [15] from a region where photoreceptors are either absent or present and degenerated beyond rescue. At 69 transitions to atrophy in 13 GA eyes, 49.3% of ELM descents were curved, 31.0% were oblique, 16.9% were reflected, and 2.8% were indeterminate due to tissue imperfections. In the last case, the ELM was extrapolated over the imperfection to Bruch's membrane.

RPE morphology on either side of the ELM descent in 13 GA eyes is illustrated microscopically in Figure 3 and graphically in Figure 4. Along this gradient RPE overall becomes increasingly non-uniform in morphology then 'sloughed'. Inside the atrophic area are 'dissociated' RPE cells lying atop BLamD. A thin layer of BLamD continues inside GA far from the ELM descent. In Figure 3A,B, flattened or dome-shaped 'subducted cells' lie on Bruch membrane throughout the atrophic area. Figure 4 shows that as the ELM descent is approached from the non-atrophic side, the percentage of abnormal RPE represented by 'sloughed', 'shedding', and 'intraretinal' morphologies increases, and the percentage of age-normal 'non-uniform' cells decreases. 'Dissociated' RPE left by the breakup of the layer are

common in atrophic zone, especially near the ELM descent. ‘Atrophy with BLamD’ is the most frequent grade at +500 μm. ‘Subducted’ cells appear on both sides of the ELM descent.

Tables 2 and 3 show thickness of the RPE layer and BLamD in relation to the ELM descent. Table 2 shows mean thicknesses for each RPE phenotype at −500 and −100 μm from this boundary. For ‘shedding’, ‘bilaminar’, and ‘intraretinal’ phenotypes, RPE was significantly thicker at −100 μm from the ELM descent than at −500 μm. ‘Sloughed’ RPE was not significantly different at the two locations, likely due to the variability in its measurement (see Methods). ‘Non-uniform’ RPE was thinner at −100 μm than at −500 μm. Combining all morphologies, RPE was 20.6% thicker at −100 μm from the ELM descent than at −500 μm (14.6 μm vs 12.1 μm), a significant difference (p=0.039). Table 3 shows that BLamD was significantly thicker at −500 μm than −100 μm for ‘sloughed’ and ‘bilaminar’ RPE and similar at both locations for other morphologies and for all morphologies combined (7.2 ± 6.1 μm vs 8.4 ± 8.2 μm, p<0.26). Although variable, the thickest BLamD was associated with ‘shedding’ RPE at −100 μm (16.7 μm) and with ‘dissociated’ RPE at +500 μm (13.9 μm). In the atrophic area, BLamD without RPE was significantly thinner far from the ELM descent (5.2 μm) than near (7.1 μm), and BLamD with ‘dissociated’ RPE did not thin at these locations (8.7 μm vs 13.9 μm, p = 0.42).

To facilitate analysis of SDOCT scans in which BLamD may not be easily separated from RPE, thicknesses for RPE and BLamD together are shown in Table 4. Combining across all RPE morphologies, RPE + BLamD is 19.6% thicker at −100 μm than at −500 μm (23.1 ± 10.7 μm vs 19.3 ± 8.2 μm), a significant difference (p=0.05).

Discussion

High-resolution clinical imaging has prompted new attention to RPE fate in GA. Based on clinical imaging studies, investigators have proposed cell death mechanisms such as lipofuscin accumulation, [36–39] necrosis, [18, 40] oxidative damage due to increased phagocytosis of damaged photoreceptors, [41, 42] and toxic molecules spreading outward from atrophy. [43, 44] To test a recently proposed two-pathway hypothesis of RPE fate in advanced AMD (apoptosis and migration) based on histology, we determined how RPE morphologies distributed across the transition from health to atrophy. Our data show a progression of RPE phenotypes toward the ELM descent in eyes with GA. Despite some individually thin cells, the net effect was overall thickening of the RPE layer. Along with showing ‘dissociated’ cells inside atrophy and ‘subducted’ cells on both sides of the ELM descent, our data support the overall hypothesis. Our results (summarized schematically in Figure 5) have several points of significance.

Biometric methods of analysis

Our report advances the histopathologic literature on GA (Supplementary Table 1) by focusing on the RPE layer as a basis for seeking associations among all chorioretinal layers in future studies. Understanding and treating GA depends critically on understanding RPE fate in a manner that matches the comprehensiveness of structural OCT imaging and adds value to FAF imaging. Foundational literature (Supplementary Table 1) established that GA, neovascularization, and drusen are part of the same age-related disease process, [45] and that

GA involves an area of RPE loss. [27, 45, 46] Early studies reported results on a per eye basis. [27, 45] Later studies introduced degrees of RPE loss [47] and a simple RPE staging system [16] to provide cellular detail and permit comparison among layers [17]. Here we used epoxy sections for a high-resolution, comprehensive, and polychromatic visualization across the whole macula. We focused on cardinal features of RPE ultrastructure, particularly spindle-shaped melanosomes and contact with a basal lamina or BLamD. The clinical variability of border features is postulated to result from different etiologies (primary atrophy, drusen-related atrophy, and atrophy after RPE detachment). [48] Using principles of unbiased systematic sampling, [49] we converted continuous variation in morphology and location to discrete categories and developed measures amenable to biometric analysis and hypothesis-testing. We included both progression to RPE cell death outside atrophic areas and for the first time, clearing processes within atrophic areas. Previous GA progression studies from our group and others classified RPE morphology in zones of different lengths along Bruch's membrane. [14, 50–52] Here we annotated RPE status at standard locations specified with respect to an origin (ELM descent). This process is less subjective and faster than finding boundaries. Thus, it is potentially applicable to SDOCT B-scans.

Pathogenic mechanisms

The GA transition has been the focus of numerous histologic studies (Supplementary Table 1) that described cells in the subretinal space as hyperplastic, hypertrophic, shed, and sloughed RPE [8, 14, 15, 18, 52, 53]. Accordingly, the SDOCT literature reports "reflective material" associated with the RPE-Bruch's membrane band, "irregular elevation of RPE", and "RPE thickening" at this junction. [26, 38, 39, 48, 54, 55]. Reports of RPE thinning [56–58] were not supported. Cells are variably identified among these authors, including RPE [48], RPE packed with pigment granules [4, 6, 54, 55], RPE/macrophages [38], and melanin-containing cells. [59] Like others using electron microscopy, we considered these subretinal cells RPE, because they contained numerous RPE-characteristic granules at a concentration resembling that of cells in the RPE layer [8, 18] and because evidence for other cell types was lacking.

We confirmed and extended earlier semi-quantitative [14] and qualitative [18] research showing dramatic changes in RPE health within 500 μm of the atrophy border. While some cells are likely dying via apoptosis ('shedding') many others appear to be undergoing transdifferentiation to a migratory phenotype, as indicated by spherical morphology and penetration past the ELM into the retina. Cells with melanosomes between BLamD and Bruch's membrane [7, 18] ('subducted') were speculated to have originated in the atrophic area as 'dissociated' cells that underwent epithelial mesenchyme transition and migrated horizontally into less affected areas, perhaps even contributing to the expansion of GA. Our new data are consistent with this model, as 'subducted' cells were proportionately more frequent in the atrophic area and at −100 μm than at −500 μm, although numbers are small. Both stage-specific RPE immunoreactivity suggesting activation and loss of polarity [16, 53, 60, 61] and non-stage-specific RPE immunoreactivity consistent with cell death pathways [44, 62] have been reported in GA eyes.

Notably, "melanin-filled" cells resembling 'sloughed' and 'intraretinal' RPE in GA express inflammatory markers (CD163, a haptoglobin-hemoglobin scavenger [61]). By high-resolution

histology, the organelle content of these phenotypes appears very similar to that of cells in the RPE layer, a coincidence difficult to ascribe phagocyte activity, and we like others [18] consider them RPE. Further, cells resembling 'subducted' also express monocyte markers CCR2 and CD68 and leukocyte marker CD18, as do cells in the RPE layer. [60, 63] Because we find transitional forms from 'dissociated' to 'subducted' in single intact histological sections [7], we consider 'subducted' of RPE origin. Assignment of cellular identify is complicated by loss of immunoreactivity for structural RPE markers in advanced AMD, so the presence of other cell types such as microglia remain a possibility. [64, 65]. Definitive assignment of identities in future studies should thus include quantification of RPE organelles and stable markers indicative of RPE origin as well as for monocyte origin [66] to distinguish among these competing hypotheses.

While not contradicting well-established roles of macrophages [67, 68] and inner-retina-derived microglia [61, 69, 70] in advanced AMD, our data point to a role for transdifferentiated RPE that remains to be determined. Further, whether treatments should promote survival or suppression of these cells is unknown. Answering such questions are now research priorities, with major ramifications for clinical image interpretation, therapeutic strategies, and choice of experimental model systems. The latter issue is germane, because many laboratory mouse strains have microglia in the subretinal space that could ingest debris and appear RPE-like due to AF. [70–73] An equivalent population has not yet been described in normal aged human eyes, although microglia appear in atrophic areas [61, 69, 70] and in association with advanced subretinal drusenoid deposits. [74] Alternatively, several mouse models involving targeted disruption of mechanistically diverse pathways also exhibit 'sloughed' RPE [75–80], supporting the concept that RPE stress responses are a final common pathway to multiple different stressors. What molecular signals prompt RPE to assume migratory behaviors in human GA eyes is unspecified. Presumably such signals will also confront replacement cells surgically delivered to patients with GA. [81, 82]

Interpretation of autofluorescence imaging

Our data have special significance for interpreting clinical FAF imaging of GA. Fully pigmented and nucleated RPE have been recently identified within atrophic areas by adaptive optics assisted near-infrared reflectance imaging and by histology. [8, 15, 19] We estimated that as much as 22% of atrophic areas retains 'dissociated' RPE, [8] which may help explain choriocapillaris survival in these regions. [83] We herein confirmed that these cells are AF (Figure 1) and thus can contribute signal. Imaging studies indicate that atrophic areas are not completely non-autofluorescent, especially towards the border. [6, 12, 24, 25, 39, 54, 55, 84–87] The atrophic area varies in FAF intensity, with rapid progressers exhibiting a moderate signal attributable now to cells as well as to BLamD. [88] The latter is visible on SDOCT as a split RPE/Bruch membrane complex. [89]

Of interest is how our data impact the interpretation of focal hyperautofluorescence found around GA, frequently thought of as high intracellular lipofuscin accumulation that leads to cell death. [36–39] RPE hypertrophy and migration both lengthen the summation path for exciting light through biologic fluorophores, as we previously demonstrated [14]. The current study replicates our finding of RPE dysmorphia in second set of GA eyes prepared with

higher-resolution histology and analyzed with a more comprehensive grading system. We suggest that this mechanism be considered the leading hypothesis to explain focally increased FAF in GA. Our current data do not support a widely-cited [6, 12, 25, 36–41, 84, 86, 87, 90–94] suggestion of RPE death by lipofuscin engorgement, granule dispersion, and necrosis. [18]

In contrast, our current data do synergize with other evidence that collectively prompt a re-evaluation of lipofuscin's role in AMD. In RPE flat mounts of AMD eyes, cells are seen to redistribute, aggregate, and overall lose autofluorescent granules in concert with cytoskeletal stress, as they degenerate. [9] Topographically precise longitudinal imaging in GA patients has shown that hyperAF indicates disease activity but does not predict atrophy on either a fine-grain [24] or population [95] basis. In AMD patients imaged with quantitative AF, which standardizes across populations via a fluorescent reference material in the light path, [96] FAF intensities decrease rather than increase. [97] Neither photoreceptor loss nor RPE loss in aging is topographically associated with AF increase in studies using accurate methods for macular cell counts [98, 99]. Mass spectrometric and chromatographic analysis of normal human and monkey eyes revealed that the well-studied lipofuscin component A2E and its major oxidation products are lower in macula than in periphery. [100–103] Thus, the relevance of experimental A2E loading of cultured RPE cells to achieve AMD milestones such as cell death [104] and complement dysregulation [105] can be questioned. Because the lipofuscin phototoxicity hypothesis underlies use of visual cycle modulators for AMD [106] and blue-light blocking intraocular lenses for cataract, [107, 108] our conclusions if sustained could have wide-ranging impact on therapeutic strategies for age-related eye disease.

Biomarkers for clinical trials – ELM descent

S.H. Sarks first observed that the ELM delimits atrophy, [27] and herein we characterized for the first time shapes of ELM descents. We and others [16, 109] previously observed that the ELM descent is comprised of reactive Müller cell processes extending outward to approach Bruch's membrane in areas of photoreceptor loss. Its shape in atrophy is governed by an outward and lateral extension of Müller cell processes as photoreceptors degenerate, as illustrated in published histology (Figure 2C,E of reference [16]; Figure 4C of reference [109] Figure 2C, 4C). Shorter or fewer photoreceptors due to marked atrophy will result in a descent that is straight and obliquely oriented rather than curved. Recent research about outer retinal tubulation (ORT), a neurodegenerative and gliotic process common in advanced AMD, established the continuity of the ELM from the GA border to the lumen of ORT, [32, 35]. Thus the 'reflected' descent may represent a phase of ORT formation via scrolling. Several authors early in the SDOCT era mentioned [85, 87, 92] or illustrated [41] the ELM as a boundary, even describing its curvature. [48] ELM presence is linked to preserved visual function, [39] and ELM absence is considered a robust indicator of atrophy [4, 6, 38, 54, 55]. Separately [110], and consistent with previous reports [18, 111] we will show that the proportion of 'oblique' ELM descents relative to 'curved' plus 'reflected' is significantly higher in donor eyes with neovascular AMD than in GA, likely due to exudation-related photoreceptor death. The ELM descent may thus have value as a biomarker in distinguishing between primary GA and atrophy secondary to neovascular AMD.

Strengths, limitations, conclusions

Strengths of this study were the number of GA eyes analyzed at high-resolution, a cellular phenotyping approach to make RPE degeneration as granular as possible, and unbiased sampling methods that included both progression and clearing processes. Limitations were the small number of RPE flat mounts for en face viewing, lack of flat-mounts and histology from the same donors, the small numbers of eyes representing some RPE phenotypes, and lack of clinical histories. Nevertheless, our study represents the first detailed examination of RPE morphology in the GA transition to since the epic 1988 description by Sarks et al [18]. As such we formulated new hypotheses testable in longitudinal imaging of appropriate patient populations, as well as a basis to study stage-specific changes originating outside the RPE layer. Data are expected to inform the interpretation of clinical SDOCT and FAF, mechanistic studies of RPE fate in AMD, and therapeutic strategies for RPE protection and replacement [82, 112].

Supplementary Material

Refer to Web version on PubMed Central for supplementary material.

Acknowledgments

CAC is supported by NEI EY06109 with institutional support from the EyeSight Foundation of Alabama and Research to Prevent Blindness Inc.

ECZ is supported by the University of Milan.

TA is supported by DFG (German Research Foundation) AC265/1-1, AC265/2-1.

RFS is supported by The Macula Foundation, Inc., New York, New York, USA

Acquisition of donor eyes was supported by International Retinal Research Foundation, National Eye Institute P30 EY003039, and the Arnold and Mabel Beckman Initiative for Macular Research. Creation of Project MACULA was additionally supported from the Edward N. and Della L. Thome Memorial Foundation.

We thank the Alabama Eye Bank for timely retrieval of donor eyes; donor families for their generosity; Giovanni Staurenghi MD for facilitating the participation of author ECZ;

David Fisher for graphical assistance in creating Figure 5.

References

1. Sunness JS, Margalit E, Srikumaran D, et al. The long-term natural history of geographic atrophy from age-related macular degeneration: enlargement of atrophy and implications for interventional clinical trials. Ophthalmology. 2007; 114:271–277. PMID 17270676. [PubMed: 17270676]
2. Feuer WJ, Yehoshua Z, Gregori G, et al. Square root transformation of geographic atrophy area measurements to eliminate dependence of growth rates on baseline lesion measurements: a reanalysis of age-related eye disease study report no. 26. JAMA Ophthalmol. 2013; 131:110–111. PMID 23307222. [PubMed: 23307222]
3. Klein ML, Ferris FL 3rd, Armstrong J, et al. Retinal precursors and the development of geographic atrophy in age-related macular degeneration. Ophthalmology. 2008; 115:1026–1031. PMID 17981333. [PubMed: 17981333]
4. Sayegh RG, Simader C, Scheschy U, et al. A systematic comparison of spectral-domain optical coherence tomography and fundus autofluorescence in patients with geographic atrophy. Ophthalmology. 2011; 118:1844–1851. PMID 21496928. [PubMed: 21496928]

5. Wu Z, Luu CD, Ayton LN, et al. Optical coherence tomography-defined changes preceding the development of drusen-associated atrophy in age-related macular degeneration. Ophthalmology. 2014; 121:2415–2422. PMID 25109931. [PubMed: 25109931]
6. Wu Z, Luu CD, Ayton LN, et al. Fundus autofluorescence characteristics of nascent geographic atrophy in age-related macular degeneration. Invest Ophthalmol Vis Sci. 2015; 56:1546–1552. PMID 25678689. [PubMed: 25678689]
7. Zanzottera EC, Messinger JD, Ach T, et al. Subducted and melanotic cells in advanced age-related macular degeneration are derived from retinal pigment epithelium. Invest Ophthalmol Vis Sci. 2015; 56:3269–3278. PMID 26024109. [PubMed: 26024109]
8. Zanzottera EC, Messinger JD, Ach T, et al. The Project MACULA retinal pigment epithelium grading system for histology and optical coherence tomography in age-related macular degeneration. Invest Ophthalmol Vis Sci. 2015; 56:3253–3268. PMID 25813989. [PubMed: 25813989]
9. Ach T, Tolstik E, Messinger JD, et al. Lipofuscin redistribution and loss accompanied by cytoskeletal stress in retinal pigment epithelium of eyes with age-related macular degeneration. Invest Ophthalmol Vis Sci. 2015; 56:3242–3252. PMID 25758814. [PubMed: 25758814]
10. Ng KP, Gugiu B, Renganathan K, et al. Retinal pigment epithelium lipofuscin proteomics. Mol Cell Proteomics. 2008; 7:1397–1405. PMID 18436525. [PubMed: 18436525]
11. Sparrow JR, Yoon KD, Wu Y, Yamamoto K. Interpretations of fundus autofluorescence from studies of the bisretinoids of the retina. Invest Ophthalmol Vis Sci. 2010; 51:4351–4357. PMID 20805567. [PubMed: 20805567]
12. Holz FG, Bindewald-Wittich A, Fleckenstein M, et al. Progression of geographic atrophy and impact of fundus autofluorescence patterns in age-related macular degeneration. Am J Ophthalmol. 2007; 143:463–472. PMID 17239336. [PubMed: 17239336]
13. Schmitz-Valckenberg S, Sahel JA, Danis R, et al. Natural history of geographic atrophy progression secondary to age-related macular degeneration (Geographic Atrophy Progression study). Ophthalmology. 2016; 123:361–368. PMID 26545317. [PubMed: 26545317]
14. Rudolf M, Vogt SD, Curcio CA, et al. Histologic basis of variations in retinal pigment epithelium autofluorescence in eyes with geographic atrophy. Ophthalmology. 2013; 120:821–828. PMID 23357621. [PubMed: 23357621]
15. Bird AC, Phillips RL, Hageman GS. Geographic atrophy: a histopathological assessment. JAMA Ophthalmol. 2014; 132:338–345. PMID 24626824. [PubMed: 24626824]
16. Guidry C, Medeiros NE, Curcio CA. Phenotypic variation of retinal pigment epithelium in age-related macular degeneration. Invest Ophthalmol Vis Sci. 2002; 43:267–273. PMID 11773041. [PubMed: 11773041]
17. Vogt SD, Curcio CA, Wang L, et al. Retinal pigment epithelial expression of complement regulator CD46 is altered early in the course of geographic atrophy. Exp Eye Res. 2011; 93:413–423. PMID 21684273. [PubMed: 21684273]
18. Sarks JP, Sarks SH, Killingsworth MC. Evolution of geographic atrophy of the retinal pigment epithelium. Eye. 1988; 2:552–577. PMID 2476333. [PubMed: 2476333]
19. Gocho K, Sarda V, Falah S, et al. Adaptive optics imaging of geographic atrophy. Invest Ophthalmol Vis Sci. 2013; 54:3673–3680. PMID 23620431. [PubMed: 23620431]
20. Pang CE, Messinger JD, Zanzottera EC, et al. The Onion Sign in neovascular age-related macular degeneration represents cholesterol crystals. Ophthalmology. 2015; 122:2316–2326. PMID 26298717. [PubMed: 26298717]
21. Chen KC, Jung JJ, Curcio CA, et al. Intraretinal hyperreflective foci in acquired vitelliform lesions of the macula: clinical and histologic study. Am J Ophthalmol. 2016; 164:89–98. PMID 26868959. [PubMed: 26868959]
22. Curcio CA, Medeiros NE, Millican CL. The Alabama age-related macular degeneration grading system for donor eyes. Invest. Ophthalmol. Vis. Sci. 1998; 39:1085–1096. PMID 9620067. [PubMed: 9620067]
23. Ach T, Huisingh C, McGwin G Jr, et al. Quantitative autofluorescence and cell density maps of the human retinal pigment epithelium. Invest Ophthalmol Vis Sci. 2014; 55:4832–4841. PMID 25034602. [PubMed: 25034602]

24. Hwang JC, Chan JW, Chang S, Smith RT. Predictive value of fundus autofluorescence for development of geographic atrophy in age-related macular degeneration. Invest Ophthalmol Vis Sci. 2006; 47:2655–2661. PMID 16723483. [PubMed: 16723483]
25. Bearelly S, Khanifar AA, Lederer DE, et al. Use of fundus autofluorescence images to predict geographic atrophy progression. Retina. 2011; 31:81–86. PMID 20890245. [PubMed: 20890245]
26. Moussa K, Lee JY, Stinnett SS, Jaffe GJ. Spectral domain optical coherence tomography-determined morphologic predictors of age-related macular degeneration-associated geographic atrophy progression. Retina. 2013; 33:1590–1599. PMID 23538573. [PubMed: 23538573]
27. Sarks SH. Ageing degeneration in the macular region: a clinico-pathological study. Br. J. Ophthalmol. 1976; 60:324–341. PMID 952802. [PubMed: 952802]
28. Uga S, Smelser. Comparative study of the fine structure of retinal Muller cells in various vertebrates. Invest Ophthalmol. 1973; 12:434–448. PMID 4541022. [PubMed: 4541022]
29. Williams DS, Arikawa K, Paallysaho T. Cytoskeletal components of the adherens junctions between the photoreceptors and the supportive Muller cells. J Comp Neurol. 1990; 295:155–164. PMID 2341633. [PubMed: 2341633]
30. Omri S, Omri B, Savoldelli M, et al. The outer limiting membrane (OLM) revisited: clinical implications. Clin Ophthalmol. 2010; 4:183–195. PMID 20463783. [PubMed: 20463783]
31. Bunt-Milam AH, Saari JC, Klock IB, Garwin GS. Zonula adherentes pore size in the external limiting membrane of the rabbit retina. Invest. Ophthalmol. Vis. Sci. 1985; 26:1377–1380. PMID 4044165. [PubMed: 4044165]
32. Schaal KB, Freund KB, Litts KM, et al. Outer retinal tubulation in advanced age-related macular degeneration: optical coherence tomographic findings correspond to histology. Retina. 2015; 35:1339–1350. PMID 25635579. [PubMed: 25635579]
33. Zweifel SA, Engelbert M, Laud K, et al. Outer retinal tubulation: a novel optical coherence tomography finding. Arch Ophthalmol. 2009; 127:1596–1602. PMID 20008714. [PubMed: 20008714]
34. Wolff B, Matet A, Vasseur V, et al. En face OCT imaging for the diagnosis of outer retinal tubulations in age-related macular degeneration. J Ophthalmol. 2012; 2012:542417. PMID 22970349. [PubMed: 22970349]
35. Litts KM, Messinger JD, Dellatorre K, et al. Clinicopathological correlation of outer retinal tubulation in age-related macular degeneration. JAMA Ophthalmol. 2015; 133:609–612. PMID 25742505. [PubMed: 25742505]
36. Schmitz-Valckenberg S, Bultmann S, Dreyhaupt J, et al. Fundus autofluorescence and fundus perimetry in the junctional zone of geographic atrophy in patients with age-related macular degeneration. Invest Ophthalmol Vis Sci. 2004; 45:4470–4476. PMID 15557456. [PubMed: 15557456]
37. Schmitz-Valckenberg S, Bindewald-Wittich A, Dolar-Szczasny J, et al. Correlation between the area of increased autofluorescence surrounding geographic atrophy and disease progression in patients with AMD. Invest Ophthalmol Vis Sci. 2006; 47:2648–2654. PMID 16723482. [PubMed: 16723482]
38. Wolf-Schnurrbusch UE, Enzmann V, Brinkmann CK, Wolf S. Morphologic changes in patients with geographic atrophy assessed with a novel spectral OCT-SLO combination. Invest Ophthalmol Vis Sci. 2008; 49:3095–3099. PMID 18378583. [PubMed: 18378583]
39. Panorgias A, Zawadzki RJ, Capps AG, et al. Multimodal assessment of microscopic morphology and retinal function in patients with geographic atrophy. Invest Ophthalmol Vis Sci. 2013; 54:4372–4384. PMID 23696601. [PubMed: 23696601]
40. Bressler, SB., Bressler, NM. Age-Related Macular Degeneration: Non-neovascular Early AMD, Intermediate AMD, and Geographic Atrophy. Retina Fifth Ryan, SJ.Schachat, AP.Wilkinson, CP., et al., editors. London: Elsevier; 2013. p. 1150-1182.
41. Schmitz-Valckenberg S, Fleckenstein M, Helb HM, et al. In vivo imaging of foveal sparing in geographic atrophy secondary to age-related macular degeneration. Invest Ophthalmol Vis Sci. 2009; 50:3915–3921. PMID 19339734. [PubMed: 19339734]
42. Pilotto E, Vujosevic S, Melis R, et al. Short wavelength fundus autofluorescence versus near-infrared fundus autofluorescence, with microperimetric correspondence, in patients with

geographic atrophy due to age-related macular degeneration. The British journal of ophthalmology. 2011; 95:1140–1144. PMID 20974627. [PubMed: 20974627]

43. Biarnés M, Monés J, Alonso J, Arias L. Update on geographic atrophy in age-related macular degeneration. Optometry and vision science : official publication of the American Academy of Optometry. 2011; 88:881–889. PMID 21532519. [PubMed: 21532519]
44. Kaneko H, Dridi S, Tarallo V, et al. DICER1 deficit induces Alu RNA toxicity in age-related macular degeneration. Nature. 2011; 471:325–330. PMID 21297615. [PubMed: 21297615]
45. Green WR, Key SN 3rd. Senile macular degeneration: a histopathologic study. Trans Am Ophthalmol Soc. 1977; 75:180–254. PMID 613523. [PubMed: 613523]
46. Gass, JDM. Diagnosis and Treatment. Saint Louis: The C. V. Mosby Company; 1977. Stereoscopic Atlas of Macular Diseases.
47. Kim SY, Sadda S, Humayun MS, et al. Morphometric analysis of the macula in eyes with geographic atrophy due to age-related macular degeneration. Retina. 2002; 22:464–470. PMID 12172114. [PubMed: 12172114]
48. Fleckenstein M, Charbel Issa P, Helb HM, et al. High-resolution spectral domain-OCT imaging in geographic atrophy associated with age-related macular degeneration. Invest Ophthalmol Vis Sci. 2008; 49:4137–4144. PMID 18487363. [PubMed: 18487363]
49. Gundersen HJG, Jensen EB. The efficiency of systematic sampling in stereology and its prediction. J. Microscopy. 1987; 147:229–263. PMID.
50. Curcio CA, Saunders PL, Younger PW, Malek G. Peripapillary chorioretinal atrophy: Bruch's membrane changes and photoreceptor loss. Ophthalmology. 2000; 107:334–343. PMID 10690836. [PubMed: 10690836]
51. Vogt SD, Curcio CA, Wang L, et al. Retinal pigment epithelial expression of complement regulator CD46 is altered early in the course of geographic atrophy. Exp Eye Res. 2011; 93:413–423. PMID 21684273. [PubMed: 21684273]
52. Biesemeier A, Taubitz T, Julien S, et al. Choriocapillaris breakdown precedes retinal degeneration in age-related macular degeneration. Neurobiol Aging. 2014; 35:2562–2573. PMID 24925811. [PubMed: 24925811]
53. Vogt SD, Curcio CA, Wang L, et al. Altered retinal pigment epithelium morphology is associated with decreased expression of complement regulatory protein CD46 and ion transporter MCT3 in geographic atrophy of age-related maculopathy. Invest Ophthalmol Vis Sci. 2009 E-abstract: 4180. PMID not available.
54. Schmitz-Valckenberg S, Fleckenstein M, Gobel AP, et al. Optical coherence tomography and autofluorescence findings in areas with geographic atrophy due to age-related macular degeneration. Invest Ophthalmol Vis Sci. 2011; 51:1–6. PMID 20688734.
55. Simader C, Sayegh RG, Montuoro A, et al. A longitudinal comparison of spectral-domain optical coherence tomography and fundus autofluorescence in geographic atrophy. Am J Ophthalmol. 2014; 158:557–66e1. PMID 24879944. [PubMed: 24879944]
56. Monés J, Biarnes M, Trindade F. Hyporeflective wedge-shaped band in geographic atrophy secondary to age-related macular degeneration: an underreported finding. Ophthalmology. 2012; 119:1412–1419. PMID 22440276. [PubMed: 22440276]
57. Sadiq MA, Hanout M, Sarwar S, et al. Structural characteristics of retinal layers adjacent to geographic atrophy. Ophthalmic Surg Lasers Imaging Retina. 2015; 46:914–919. PMID 26469230. [PubMed: 26469230]
58. Folgar FA, Yuan EL, Sevilla MB, et al. Drusen volume and retinal pigment epithelium abnormal thinning volume predict 2-year progression of age-related macular degeneration. Ophthalmology. 2016; 123:39 e1–50 e1. PMID 26578448. [PubMed: 26578448]
59. Querques G, Kamami-Levy C, Georges A, et al. Adaptive optics imaging of foveal sparing in geographic atrophy secondary to age-related macular degeneration. Retina. 2016; 36:247–254. PMID 26200512. [PubMed: 26200512]
60. Sennlaub F, Auvynet C, Calippe B, et al. CCR2(+) monocytes infiltrate atrophic lesions in age-related macular disease and mediate photoreceptor degeneration in experimental subretinal inflammation in Cx3cr1 deficient mice. EMBO Mol Med. 2013; 5:1775–1793. PMID 24142887. [PubMed: 24142887]

61. Lad EM, Cousins SW, Van Arnam JS, Proia AD. Abundance of infiltrating CD163+ cells in the retina of postmortem eyes with dry and neovascular age-related macular degeneration. Graefes Arch Clin Exp Ophthalmol. 2015 PMID 26148801.
62. Kim Y, Tarallo V, Kerur N, et al. DICER1/Alu RNA dysmetabolism induces Caspase-8-mediated cell death in age-related macular degeneration. Proc Natl Acad Sci U S A. 2014; 111:16082–16087. PMID 25349431. [PubMed: 25349431]
63. Cherepanoff S, McMenamin PG, Gillies MC, et al. Bruch's membrane and choroidal macrophages in early and advanced age-related macular degeneration. Br J Ophthalmol. 2010; 94:918–925. PMID 19965817. [PubMed: 19965817]
64. Lad EM, Cousins SW, Proia AD. Identity of pigmented subretinal cells in age-related macular degeneration. Graefes Arch Clin Exp Ophthalmol. 2016; 254:1239–1241. PMID 26728757. [PubMed: 26728757]
65. Fuchs U, Kivelä T, Tarkkanen A. Cytoskeleton in normal and reactive human retinal pigment epithelial cells. Invest. Ophthalmol. Vis. Sci. 1991; 32:3178–3186. PMID 1748549. [PubMed: 1748549]
66. Curcio CA, Ach T, et al. Macrophages or retinal pigment epithelium expressing macrophage markers in age-related macular degeneration? Comment on Lad et al. 2015. Graefes Arch Clin Exp Ophthalmol. 2016; 254:1237–1238. PMID 26897741. [PubMed: 26897741]
67. Sarks JP, Sarks SH, Killingsworth MC. Morphology of early choroidal neovascularization in age-related macular degeneration: correlation with activity. Eye. 1997; 11:515–522. PMID 9425418. [PubMed: 9425418]
68. Grossniklaus HE, Cingle KA, Yoon YD, et al. Correlation of histologic 2-dimensional reconstructional and confocal scanning laser microscopic imaging of choroidal neovascularization in eyes with age-related maculopathy. Arch Ophthalmol. 2000; 118:625–629. PMID 10815153. [PubMed: 10815153]
69. Gupta N, Brown KE, Milam AH. Activated microglia in human retinitis pigmentosa, late-onset retinal degeneration, and age-related macular degeneration. Exp Eye Res. 2003; 76:463–471. PMID 12634111. [PubMed: 12634111]
70. Ma W, Coon S, Zhao L, et al. A2E accumulation influences retinal microglial activation and complement regulation. Neurobiol Aging. 2013; 34:943–960. PMID 22819137. [PubMed: 22819137]
71. Xu H, Chen M, Manivannan A, et al. Age-dependent accumulation of lipofuscin in perivascular and subretinal microglia in experimental mice. Aging Cell. 2008; 7:58–68. PMID 17988243. [PubMed: 17988243]
72. Combadière C, Feumi C, Raoul W, et al. CX3CR1-dependent subretinal microglia cell accumulation is associated with cardinal features of age-related macular degeneration. J Clin Invest. 2007; 117:2920–2928. PMID 17909628. [PubMed: 17909628]
73. Chen M, Forrester JV, Xu H. Dysregulation in retinal para-inflammation and age-related retinal degeneration in CCL2 or CCR2 deficient mice. PLoS ONE. 2011; 123:1320–1331. PMID 21850237.
74. Greferath U, Guymer R. Correlation of histologic features with in vivo imaging of reticular pseudodrusen. Ophthalmology. 2016 PMID.
75. Hahn P, Qian Y, Dentchev T, et al. Disruption of ceruloplasmin and hephaestin in mice causes retinal iron overload and retinal degeneration with features of age-related macular degeneration. Proc Natl Acad Sci U S A. 2004; 101:13850–13855. Epub 2004 Sep 13. PMID 15365174. [PubMed: 15365174]
76. Zhao C, Yasumura D, Li X, et al. mTOR-mediated dedifferentiation of the retinal pigment epithelium initiates photoreceptor degeneration in mice. J Clin Invest. 2011; 121:369–383. PMID 21135502. [PubMed: 21135502]
77. Patil H, Saha A, Senda E, et al. Selective impairment of a subset of Ran-GTP-binding domains of ran-binding protein 2 (Ranbp2) suffices to recapitulate the degeneration of the retinal pigment epithelium (RPE) triggered by Ranbp2 ablation. J Biol Chem. 2014; 289:29767–29789. PMID 25187515. [PubMed: 25187515]

78. Collin GB, Hubmacher D, Charette JR, et al. Disruption of murine ADAMTSL4 results in zonular fiber detachment from the lens and retinal pigment epithelium dedifferentiation. Hum Mol Genet. 2015; 24:6958–6974. PMID 26405179. [PubMed: 26405179]

79. Jadeja S, Barnard AR, McKie L, et al. Mouse slc9a8 mutants exhibit retinal defects due to retinal pigmented epithelium dysfunction. Invest Ophthalmol Vis Sci. 2015; 56:3015–3026. PMID 25736793. [PubMed: 25736793]

80. Saksens NT, Krebs MP, Schoenmaker-Koller FE, et al. Mutations in CTNNA1 cause butterfly-shaped pigment dystrophy and perturbed retinal pigment epithelium integrity. Nat Genet. 2016; 48:144–151. PMID 26691986. [PubMed: 26691986]

81. Schwartz SD, Regillo CD, Lam BL, et al. Human embryonic stem cell-derived retinal pigment epithelium in patients with age-related macular degeneration and Stargardt's macular dystrophy: follow-up of two open-label phase 1/2 studies. Lancet. 2014; 385:509–516. PMID 25458728. [PubMed: 25458728]

82. Nazari H, Zhang L, Zhu D, et al. Stem cell based therapies for age-related macular degeneration: The promises and the challenges. Prog Retin Eye Res. 2015; 48:1–39. PMID 26113213. [PubMed: 26113213]

83. Giani A, Pellegrini M, Carini E, et al. The dark atrophy with indocyanine green angiography in Stargardt disease. Invest Ophthalmol Vis Sci. 2012; 53:3999–4004. PMID 22589445. [PubMed: 22589445]

84. Bindewald A, Schmitz-Valckenberg S, Jorzik JJ, et al. Classification of abnormal fundus autofluorescence patterns in the junctional zone of geographic atrophy in patients with age related macular degeneration. Br J Ophthalmol. 2005; 89:874–878. PMID 15965170. [PubMed: 15965170]

85. Brar M, Kozak I, Cheng L, et al. Correlation between spectral-domain optical coherence tomography and fundus autofluorescence at the margins of geographic atrophy. Am J Ophthalmol. 2009; 148:439–444. PMID 19541290. [PubMed: 19541290]

86. Biarnés M, Monés J, Trindade F, et al. Intra and interobserver agreement in the classification of fundus autofluorescence patterns in geographic atrophy secondary to age-related macular degeneration. Graefe's archive for clinical and experimental ophthalmology = Albrecht von Graefes Archiv fur klinische und experimentelle Ophthalmologie. 2011; 250:485–490. PMID 22033626.

87. Göbel AP, Fleckenstein M, Schmitz-Valckenberg S, et al. Imaging geographic atrophy in age-related macular degeneration. Ophthalmologica. Journal international d'ophtalmologie. International journal of ophthalmology. Zeitschrift fur Augenheilkunde. 2011; 226:182–190. PMID 21865677. [PubMed: 21865677]

88. Ooto S, Vongkulsiri S, Sato T, et al. Outer retinal corrugations in age-related macular degeneration. JAMA Ophthalmol. 2014; 132:806–813. PMID 24801396. [PubMed: 24801396]

89. Fleckenstein M, Schmitz-Valckenberg S, Lindner M, et al. The "diffuse-trickling" fundus autofluorescence phenotype in geographic atrophy. Invest Ophthalmol Vis Sci. 2014; 55:2911–2920. PMID 24699379. [PubMed: 24699379]

90. Holz F, Bellmann C, Margaritidis M, et al. Patterns of increased in vivo fundus autofluorescence in the junctional zone of geographic atrophy of the retinal pigment epithelium associated with age-related macular degeneration. Graefes. Arch. Clin. Exp. Ophthalmol. 1999; 237:145–152. PMID 9987631. [PubMed: 9987631]

91. Holz FG, Bellman C, Staudt S, et al. Fundus autofluorescence and development of geographic atrophy in age-related macular degeneration. Investigative Ophthalmology & Visual Science. 2001; 42:1051–1056. PMID 11274085. [PubMed: 11274085]

92. Bearelly S, Chau FY, Koreishi A, et al. Spectral domain optical coherence tomography imaging of geographic atrophy margins. Ophthalmology. 2009; 116:1762–1769. PMID 19643488. [PubMed: 19643488]

93. Holz FG, Strauss EC, Schmitz-Valckenberg S, van Lookeren Campagne M. Geographic atrophy: clinical features and potential therapeutic approaches. Ophthalmology. 2014; 121:1079–1091. PMID 24433969. [PubMed: 24433969]

94. Yehoshua Z, de Amorim Garcia Filho CA, Nunes RP, et al. Comparison of geographic atrophy growth rates using different imaging modalities in the COMPLETE Study. Ophthalmic Surg Lasers Imaging Retina. 2015; 46:413–422. PMID 25970861. [PubMed: 25970861]
95. Biarnes M, Arias L, Alonso J, et al. Increased fundus autofluorescence and progression of geographic atrophy secondary to age-related macular degeneration: the GAIN study. Am J Ophthalmol. 2015; 160:345–353 e5. PMID 25982972. [PubMed: 25982972]
96. Delori F, Greenberg JP, Woods RL, et al. Quantitative measurements of autofluorescence with the scanning laser ophthalmoscope. Investigative Ophthalmology & Visual Science. 2011; 52:9379–9390. PMID 22016060. [PubMed: 22016060]
97. Gliem M, Muller PL, Finger RP, et al. Quantitative fundus autofluorescence in early and intermediate age-related macular degeneration. JAMA Ophthalmol. 2016; 134:817–824. PMID 27253610. [PubMed: 27253610]
98. Curcio CA, Millican CL, Allen KA, Kalina RE. Aging of the human photoreceptor mosaic: evidence for selective vulnerability of rods in central retina. Invest. Ophthalmol. Vis. Sci. 1993; 34:3278–3296. PMID 8225863. [PubMed: 8225863]
99. Ach T, Huisingh C, McGwin G, et al. Quantitative autofluorescence and cell density maps of the human retinal pigment epithelium. Invest Ophthalmol Vis Sci. 2014 PMID 25034602.
100. Bhosale P, Serban B, Bernstein PS. Retinal carotenoids can attenuate formation of A2E in the retinal pigment epithelium. Archives of Biochemistry and Biophysics. 2009; 483:175–181. PMID 18926795. [PubMed: 18926795]
101. Ablonczy Z, Higbee D, Anderson DM, et al. Lack of correlation between the spatial distribution of A2E and lipofuscin fluorescence in the human retinal pigment epithelium. Invest Ophthalmol Vis Sci. 2013; 54:5535–5542. PMID 23847313. [PubMed: 23847313]
102. Pallitto P, Ablonczy Z, Jones EE, et al. A2E and lipofuscin distributions in macaque retinal pigment epithelium are similar to human. Photochem Photobiol Sci. 2015; 14:1888–1895. PMID 26223373. [PubMed: 26223373]
103. Adler L, Boyer NP, Anderson DM, et al. Determination of N-retinylidene-N-retinylethanolamine (A2E) levels in central and peripheral areas of human retinal pigment epithelium. Photochem Photobiol Sci. 2015; 14:1983–1990. PMID 26323192. [PubMed: 26323192]
104. Sparrow JR, Parish CA, Hashimoto M, Nakanishi K. A2E a lipofuscin fluorophore in human retinal pigmented epithelial cells in culture. Invest. Ophthalmol. Vis. Sci. 1999; 40:2988–1995. PMID 10845625. [PubMed: 10549662]
105. Zhou J, Jang YP, Kim SR, Sparrow JR. Complement activation by photooxidation products of A2E, a lipofuscin constituent of the retinal pigment epithelium. Proceedings of the National Academy of Sciences of the United States of America. 2006; 103:16182–16187. PMID 17060630. [PubMed: 17060630]
106. Zarbin MA, Rosenfeld PJ. Pathway-based therapies for age-related macular degeneration: an integrated survey of emerging treatment alternatives. Retina. 2010; 30:1350–1367. PMID 20924259. [PubMed: 20924259]
107. Carson D, Margrain TH, Patel A. New approach to evaluate retinal protection by intraocular lenses against age-related lipofuscin accumulation-mediated retinal phototoxicity. Journal of cataract and refractive surgery. 2008; 34:1785–1792. PMID 18812134. [PubMed: 18812134]
108. Mainster MA, Turner PL. Blue-blocking IOLs vs. short-wavelength visible light: hypothesis-based vs. evidence-based medical practice. Ophthalmology. 2010; 118:1–2. PMID 21199710.
109. Wu KH, Madigan MC, Billson FA, Penfold PL. Differential expression of GFAP in early v late AMD: a quantitative analysis. Br J Ophthalmol. 2003; 87:1159–1166. PMID 12928288. [PubMed: 12928288]
110. Zanzottera EC, Ach T, Huisingh C, et al. Visualizing retinal pigment epithelium phenotypes in the transition to atrophy in neovascular age-related macular degeneration. Retina. 2016 [Epub ahead of print] PMID: 27685678.
111. Sarks J, Tang K, Killingsworth M, et al. Development of atrophy of the retinal pigment epithelium around disciform scars. Br J Ophthalmol. 2006; 90:442–446. PMID 16547324. [PubMed: 16547324]

112. Binder S, Stanzel BV, Krebs I, Glittenberg C. Transplantation of the RPE in AMD. Prog Retin Eye Res. 2007; 26:516–554. PMID 17532250. [PubMed: 17532250]

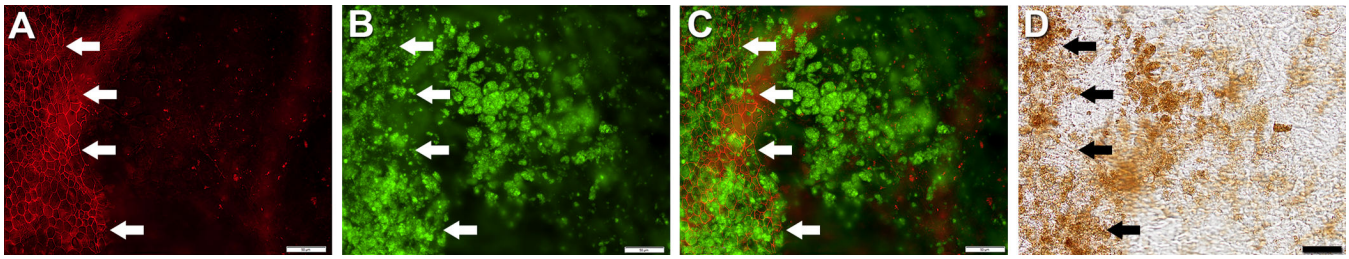

Figure 1. Variation in RPE autofluorescence and cytoskeleton in geographic atrophy

RPE-Bruch's membrane flat mount from an 81-year-old male with geographic atrophy secondary to AMD, with abundant AF material inside the atrophic area. Arrows indicate termination of organized RPE cytoskeleton in all panels. **A**. Phalloidin-labeled cytoskeleton of RPE cells at the border of atrophy. In the atrophic zone, cells lose f-actin cytoskeleton, and condensed f-actin tangles form from remaining f-actin fragments. **B**. Brightly AF lipofuscin/melanolipofuscin granules, either within isolated cells or in extracellular granule aggregates shed into basal laminar deposit [9]. **C**. Images from Panels A and B are superimposed to show the relationship of AF material to the termination of organized cytoskeleton. **D**. Bright field image confirms that cells and cellular fragments also have melanosomes. Scale bar: 50 μm.

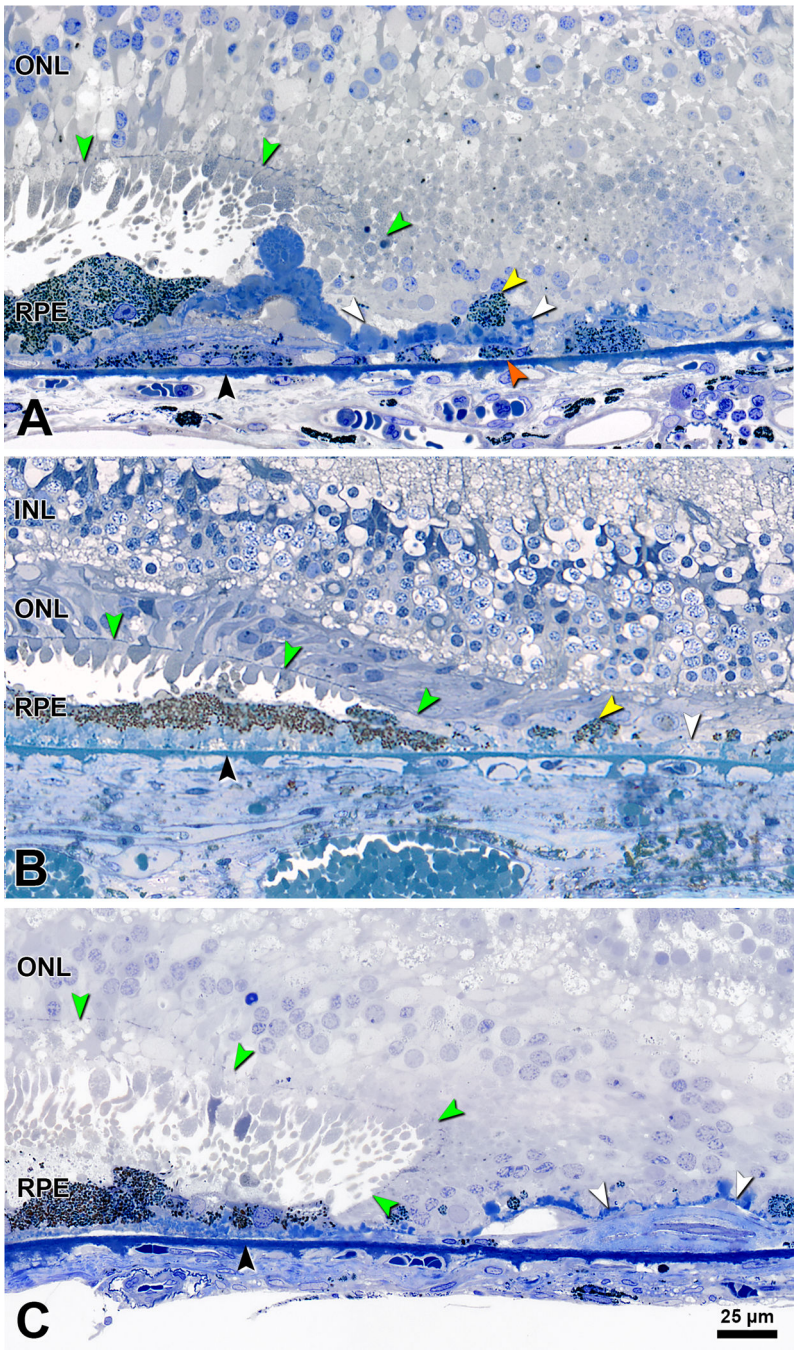

Figure 2. Descent of the external limiting membrane in 3 eyes with geographic atrophy

Panoramic views of the transition to atrophy in these eyes are shown in Figure 3. ELM, external limiting membrane, green arrowheads; INL, inner nuclear layer; ONL, outer nuclear layer; RPE, retinal pigment epithelium. Bruch's membrane, black arrowhead; persistent BLamD, white arrowhead. Bar in C applies to all panels. **A**. The ELM descent is curved. 'Dissociated' RPE, yellow arrowhead; 'subducted RPE, orange arrowhead. 87-year-old man. **B**. The ELM descent is oblique. 83-year-old woman. **C**. The ELM descent is reflected. 90-year-old-man.

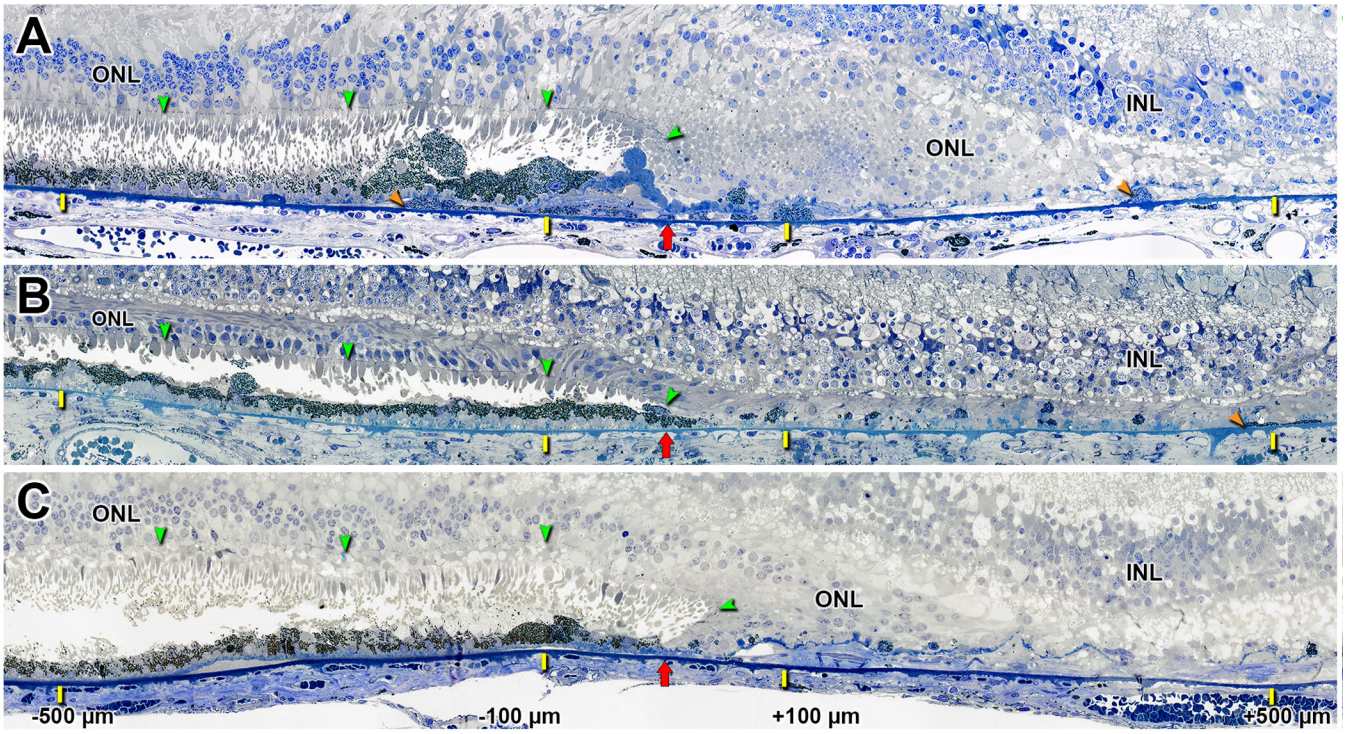

Figure 3. Retinal pigment epithelium morphology in eyes with geographic atrophy

ELM descent (green arrowheads) and its projection onto Bruch's membrane (red arrow) are shown. Regions between −100 and +100 µm are shown at higher magnification in Figure 2. RPE and BLamD morphology and thickness were analyzed at −500 and −100 µm outside GA (yellow ticks, to the left of the red arrow) and +500 and +100 µm inside GA (yellow ticks, to the right of the right arrow). Sub-micrometer epoxy sections, toluidine blue stain. INL= Inner nuclear layer, ONL= Outer nuclear layer. **A**. The ONL sweeps past the curved ELM descent, into the atrophic area. 87-year-old man. **B**. The ONL is parallel to a oblique ELM descent. 83-year-old woman. **C**. The ONL sweeps past a reflected ELM descent, into the atrophic area. 90-year-old-man. Outside GA (**A,B,C**): 'Non-uniform' RPE becomes 'Very non-uniform', then 'sloughed' in sub-retinal space, near the ELM descent. Inside GA (**A,B,C**): 'dissociated' RPE cells persist over BLamD, and a thin layer of BLamD remains far from the border. In **A** and **B**, 'Subducted' cells lie on Bruch's membrane (orange arrowhead). In **A** and **C**, one giant RPE cell at −100 µm is packed with granules[9]. Complete sections are available at Project MACULA website. A. http://projectmacula.cis.uab.edu/?p=2799; C. http://projectmacula.cis.uab.edu/?p=2288

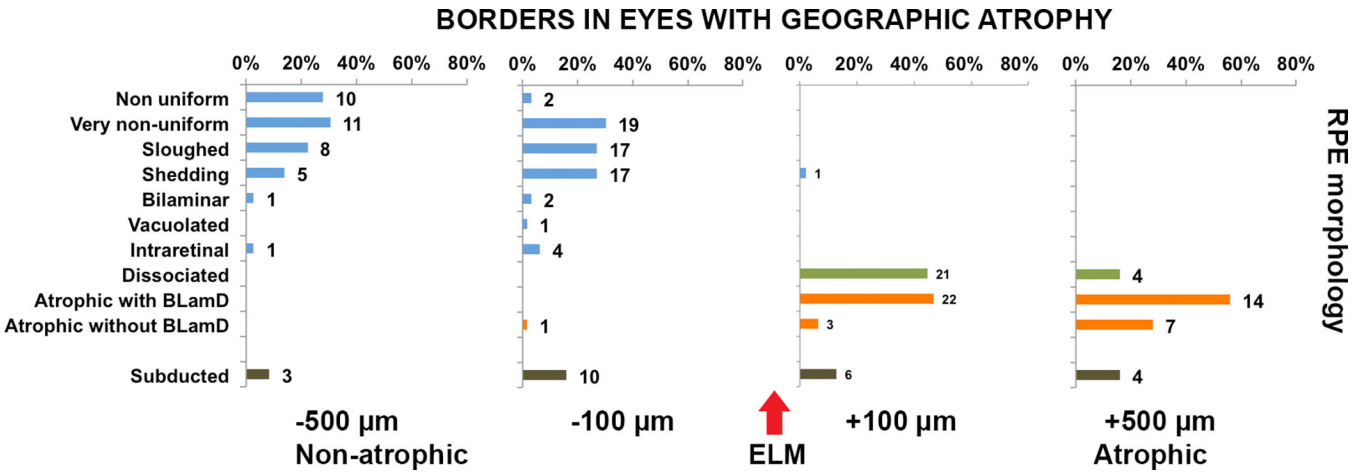

Figure 4. Distribution of RPE morphologies with respect to the ELM descent in geographic atrophy

The ELM descent defines GA margins (red arrow). The number of assessment locations is expressed at the right of each bar. Epithelial, non-epithelial, atrophic, and subducted morphologies [8] are indicated by blue, green, orange, and brown bars respectively, with less affected at the top and more affected at the bottom. Percentages are referenced to the total number of RPE. There is a shift from age-normal to abnormal RPE phenotypes at the ELM descent. We confirmed a single atrophic grade at −100 µm and epithelial grade at +100 µm.

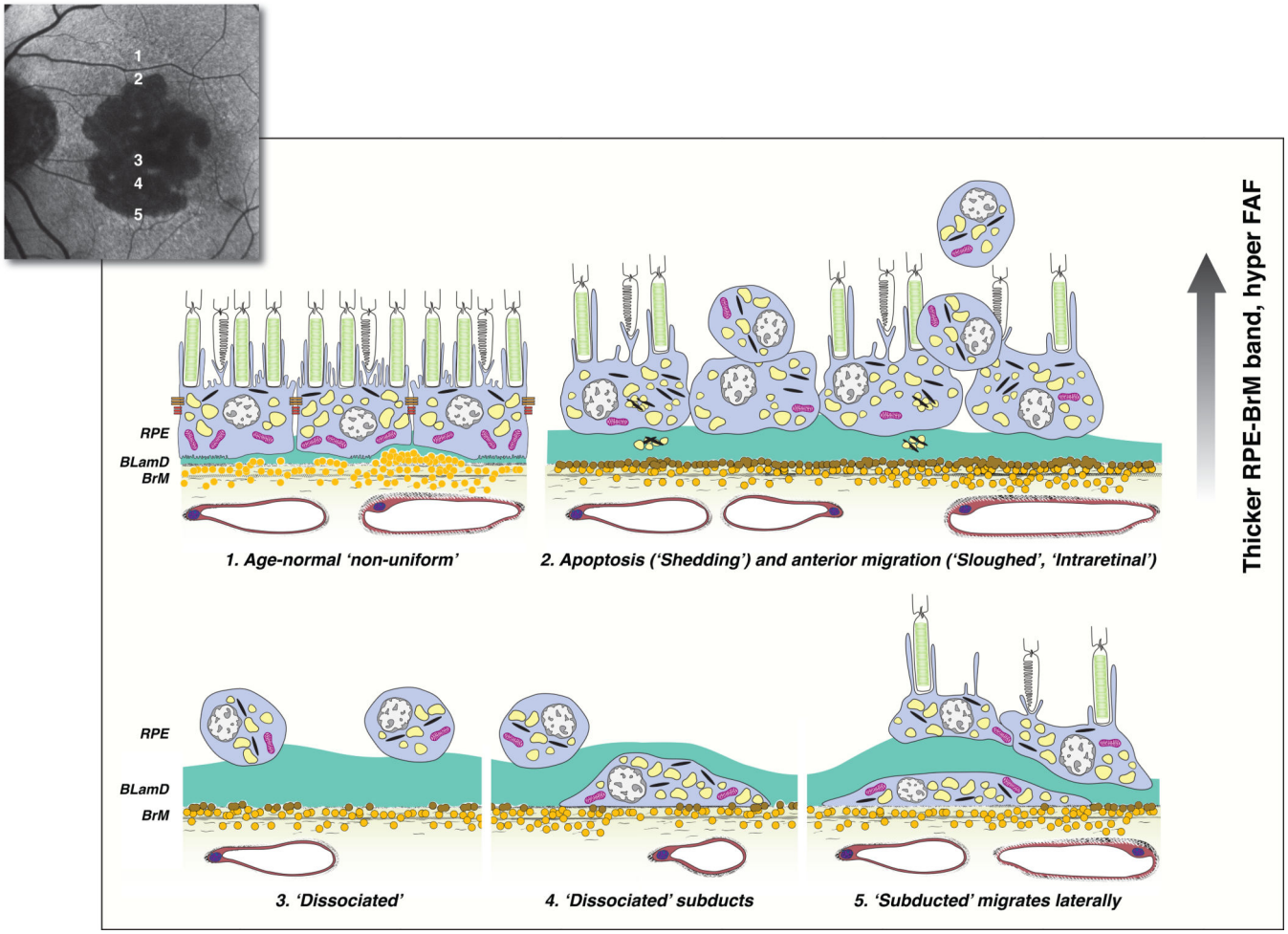

Figure 5.

Hypothesized sequence of RPE fate with imaging consequences at the border of geographic atrophy (GA) in AMD. Phenotypes of RPE morphology were previously described [7, 8]. The ELM descent is not shown. As indicated on a representative fundus autofluorescence image of a patient with GA, **panels 1–2** move from the margin of atrophy to its center. **Panels 3–5** move from the center to the margin. **1**. Age-normal 'non-uniform' RPE overlies Bruch's membrane, which contains numerous lipoprotein particles (yellow). Basal laminar deposit (BLamD, green) is thin and continuous. RPE organelles are reflective and stacked in three cushions from apical to basal - melanosomes, lipofuscin, and mitochondria. **2**. Within 500 μm of the border, cells undergo apoptosis ('shedding') and anterior migration ('sloughed' or 'intraretinal'); and BLamD is thick. The net effect of RPE dysmorphia on imaging is thickening and roughening of the hyperreflective RPE-Bruch's membrane band by SDOCT, hyperreflective foci in the retina and within thick BLamD, [8, 21] and variably focal hyperautofluorescence. **3**. Due to death or migration of RPE, the remaining layer disintegrates. Pigmented and nucleated 'dissociated' RPE are scattered across the atrophic zone and may be visible by autofluorescence. **4**. 'Subducted' cells likely originate in the atrophic zone, where they are unmoored from their junctional complexes. They dive down and flatten on Bruch's membrane while retaining a reduced number of characteristic

granules. **5**. ‘Subducted’ cells migrate at least 100 μm into the marginal area and express inflammatory markers [61, 64, 66]. While their activities are not known, they could participate in the spread of GA.

Table 1

Histological phenotypes of retinal pigment epithelium in age-related macular degeneration

RPE phenotype	**Description (grades used in previous publications [14, 17])**
Non uniform	Slightly non-uniform morphology and pigmentation (1)
Very non-uniform	Very non-uniform morphology and pigmentation (2)
Sloughed	Intact epithelium with spherical cells sloughed into sub-retinal space (2A)
Shedding	Intact epithelium with basal shedding of non-nucleated RPE fragments containing granules into basal laminar deposits (2B)
Bilaminar	Double layers (2L)
Vacuolated	A single large vacuole, sometimes with contents, delimited apically by extremely effaced cytoplasm
Intraretinal	Anterior migration of nucleated RPE through the external limiting membrane (3)
Dissociated	Nucleated RPE in atrophic area (no external limiting membrane), adherent to persistent BLamD or Bruch's membrane
Entombed	Entombed by fibrovascular scar, intermingled with other cells and fluid in the same layer
Subducted	Rounded or flattened, in sub-RPE space, not adjacent to basal lamina
Melanotic	Large black, spherical melanosomes, individual cells or cells in multiple layers, in sub-retinal or sub-RPE space, associated with neovascular scars
Entubulated	In lumen of outer retinal tubulation, not adjacent to basal lamina
Atrophy with BLamD	No cells; persistent basal laminar deposits (4)
Atrophy without BLamD	No cells; no basal laminar deposit (5)

Notes: phenotypes defined by Zanzottera et al [7, 8]

Abbreviations: BLamD, basal laminar deposits; RPE, retinal pigment epithelium.

Table 2

RPE thickness relative to the ELM descent in geographic atrophy

	−500 μm	−100 μm		Overall
RPE Morphology	**RPE thickness, μm Mean ± SD; N**	**RPE thickness, μm Mean ± SD; N**	**p-value, -500 μm vs –100 μm**	**RPE thickness, μm Mean ± SD; N**
Overall	12.1 ± 5.2; 12	14.6 ± 6.9; 12	0.039	13.7 ± 6.4; 12
Non-uniform	10.9 ± 2.5; 8	8.3 ± 0.2; 2	<0.0001	10.5 ± 2.5; 9
Very non-uniform	12.5 ± 3.2; 6	11.8 ± 4.9; 7	0.48	12.1 ± 4.3; 8
Sloughed	15.3 ± 9.3; 6	18.3 ± 7.4; 9	0.43	17.4 ± 8.0; 10
Shedding	9.0 ± 2.0; 4	14.1 ± 7.6; 7	<0.0001	13.0 ± 7.0; 8
Bilaminar	9.3 (n/a); 1	20.4 ± 11.0; 2	0.044	16.7 ± 10.0; 3
Vacuolated	---	13.2 (n/a); 1	---	13.2 (n/a); 1
Intraretinal	10.5 (n/a); 1	14.4 ± 1.5; 2	<0.0001	13.6 ± 2.2; 3

Notes:

N indicates number of donors in which measurements were made (13 eyes from 12 donors total).

Thicknesses were measured for the epithelial component of morphologies that also included a non-epithelial component, as described [8].

Thicknesses were not recorded for ‘dissociated’ RPE within the atrophic area.

P-value obtained via general estimating equations

SD, standard deviation

n/a, not applicable

Table 3

Basal laminar deposit thickness relative to the ELM descent in geographic atrophy

RPE Morphology	−500 µm from ELM descent	−100 µm from ELM descent	−500 µm vs −100 µm	+100 µm from ELM descent	+500 µm from ELM descent	+500 µm vs +100 µm	Overall -500 µm and −100 µm	Overall +100 µm and +500 µm
	BLamD thickness in µm, mean ± SD; N		*p*-value	BLamD thickness in µm, mean ± SD; N		*p*-value	BLamD thickness in µm, mean ± SD; N	
Overall	7.2 ± 6.1; 12	8.4 ± 8.2; 12	0.26	7.4 ± 5.6; 12	5.1 ± 7.0; 11	0.0784	8.0 ± 7.5; 12	6.6 ± 6.2; 12
Non-uniform	3.1 ± 3.0; 8	6.0 ± 2.7; 2	0.15	---	---	---	3.6 ± 3.0; 9	---
Very non-uniform	6.5 ± 6.6; 6	4.7 ± 5.2; 7	0.38	---	---	---	5.4 ± 5.7; 8	---
Sloughed	9.1 ± 5.2; 6	5.6 ± 2.7; 9	0.045	---	---	---	6.7 ± 3.9; 10	---
Shedding	14.6 ± 5.6; 4	16.7 ± 10.0; 7	0.29	---	---	---	16.2 ± 9.1; 8	---
Bilaminar	5.0 (n/a); 1	1.4 ± 1.9; 2	0.0001	---	---	---	2.6 ± 2.5; 3	---
Vacuolated	---	5.5 (n/a); 1	---	---	---	---	5.5 (n/a); 1	---
Intraretinal	7.3 (n/a); 1	8.9 ± 8.9; 2	0.66	---	---	---	8.6 ± 7.7; 3	---
Dissociated	---	---	---	8.7 ± 6.7; 10	13.9 ± 14.8; 4	0.42	---	9.6 ± 8.3; 10
Atrophy with BLamD	---	---	---	7.1 ± 3.6; 9	5.2 ± 1.4; 7	0.019	---	6.3 ± 3.0; 9
Atrophy Without BLamD	---	---	---	0.6 (1.1); 3	0 (n/a); 5	0.29	---	0.2 ± 0.7; 6

Notes:

N indicates number of donors in which measurements were made (13 eyes from 12 donors total).

P-value obtained via general estimating equations

Different morphologies were observed in atrophic vs. non-atrophic areas, so BLamD thickness between these areas was not compared statistically.

SD, standard deviation

n/a, not applicable

Table 4

RPE + Basal laminar deposit thickness relative to the ELM descent in geographic atrophy

RPE Morphology	−500 μm from ELM descent	−100 μm from ELM descent	−500 μm vs −100 μm	Overall
	RPE + BLamD thickness in μm, mean ± SD; N		*p*-value	RPE + BLamD thickness in μm, mean ± SD; N
Overall	19.3 ± 8.2; 12	23.1 ± 10.7; 12	0.05	21.7 ± 10.0; 12
Non-uniform	14.1 ± 2.8; 8	14.3 ± 2.5; 2	0.93	14.1 ± 2.7; 9
Very non Uniform	19.0 ± 8.7; 6	16.5 ± 7.3; 7	0.34	17.4 ± 7.8; 8
Sloughed	24.4 ± 10.2; 6	23.9 ± 7.6; 9	0.91	24.1 ± 8.3; 10
Shedding	23.6 ± 7.2; 4	30.9 ± 12.7; 7	<0.0001	29.2 ± 11.9; 8
Bilaminar	14.3 (n/a); 1	21.7 ± 12.9; 2	0.25	19.2 ± 10.1; 3
Vacuolated	---	18.7 (n/a); 1	---	18.7 (n/a); 1
Intraretinal	17.8 (n/a); 1	23.4 (10.3): 2	0.21	22.2 (9.2); 3

Notes:

N indicates the number of donors in which measurements were made (13 eyes from 12 donors total).

P-value obtained via general estimating equations

SD, standard deviation

n/a, not applicable